ULTRA WIDE SWATH IMAGING WITH MULTI-CHANNEL SCANSAR

Nicolas Gebert[1]*, Gerhard Krieger, Marwan Younis, Federica Bordoni, Alberto Moreira*

German Aerospace Center (DLR), Microwaves and Radar Institute, 82234 Wessling, Germany
[1]Phone: +49 8153 / 28 -3331, Fax: +49 8153 / 28 -1449, Email: nico.gebert@dlr.de

ABSTRACT

Multi-channel synthetic aperture radar (SAR) systems enable high-resolution wide-swath imagery thus overcoming the inherent limitation of conventional SAR. A possible realization based on the combination of multi-aperture SAR signal reconstruction in azimuth with digital beamforming on receive in elevation is given in [1]. The present paper turns focus to advanced concepts for the imaging of even wider swaths while still providing high azimuth resolution [2]. In this regard, the operation of multi-channel SAR systems in burst modes like ScanSAR or TOPS is introduced and aspects of applying the multi-aperture reconstruction algorithm to burst mode data are analyzed. The influence of the digital processing network on performance parameters as signal-to-noise-ratio and azimuth ambiguity-to-signal-ratio in multi-channel burst mode systems is considered and embedded in the design example of a ScanSAR system that allows for the imaging of a 400 km wide swath with a geometric resolution of 5 m. Finally, first results for a multi-channel TOPS system are presented and an optimized TOPS processing approach is introduced.

1. INTRODUCTION TO MULTI-CHANNEL SAR

In multi-aperture SAR systems additional information is received by the multiple channels what allows for imaging wide swaths with a high geometric resolution (cf. Fig. 1). In systems with multiple azimuth channels, a challenge is posed by a non-optimum relation between applied pulse repetition frequency (*PRF*) and spacing of the receive apertures what leads to a non-uniform spatial distribution of azimuth data samples. Such systems need additional signal processing which accomplishes independently on the *PRF* the combination of the sub-sampled input channels to a non-aliased output signal. A solution to this digital processing problem is given by the *multi-aperture reconstruction algorithm* that enables unambiguous recovery of the sub-sampled azimuth spectrum by applying to each of the system's channels a Doppler frequency f dependent filter function $P_{j,PRF}(f)$. The inverse character of this filter network may lead to a degradation of the signal-to-noise ratio (*SNR*) which is described by the *SNR* scaling factor Φ_{bf}. Further, the azimuth-ambiguity-to-signal ratio ($AASR_N$) is also influenced by the signal processing network which is hence to be taken into account to determine the $AASR_N$ in multi-channel systems.[1]

As demonstrated in [1], multi-channel SAR systems permit imaging of a swath of 100 km width with a resolution of 1 m by employing an antenna of length 11.6 m. Nevertheless, demands to future SAR systems are frequent and detailed imagery on global scale leading to a necessary swath of 400 km if weekly imaging of the whole earth is assumed. This entails a maximum allowable *PRF* of ~400 Hz which drives the minimum antenna length in azimuth, yielding an unreasonable optimum length of ~35-40 m. Hence, innovative concepts are required to enable ultra-wide-swaths with acceptable antenna dimensions. A possible solution is a multi-channel SAR system in burst mode operation which is investigated in the subsequent Sections.

2. MULTI-CHANNEL BURST MODE SAR

In burst modes like ScanSAR [3][4] or TOPS-SAR [5] the antenna footprint is switched between a number of sub-swaths, what allows for an overall swath width that consists of all sub-swaths but is at the cost of a coarsened azimuth resolution (cf. Fig. 2). This can be compensated operating multi-channel SAR in burst modes, what enables ultra-wide swaths of several hundreds of kilometres while providing a resolution well below 10 m (cf. Fig. 3, [6]).

In this regard, special interest is turned to the impact of the

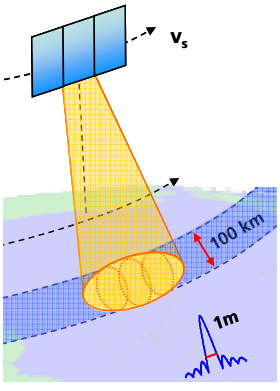

Fig. 1. High-Resolution Wide-Swath SAR System.

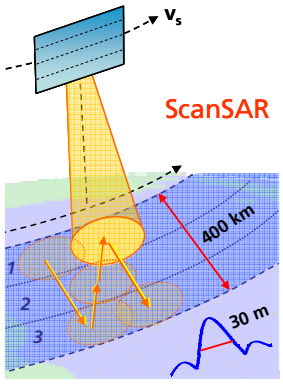

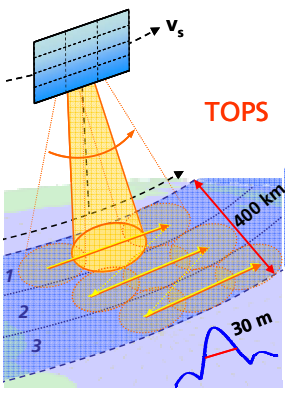

Fig. 2. Burst Mode Systems: ScanSAR (left) and TOPS (right) for ultra-wide swaths with coarse resolution.

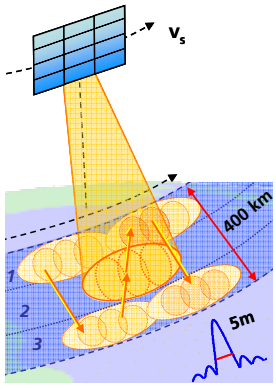

Fig. 3. Multi-Aperture Burst Mode SAR .

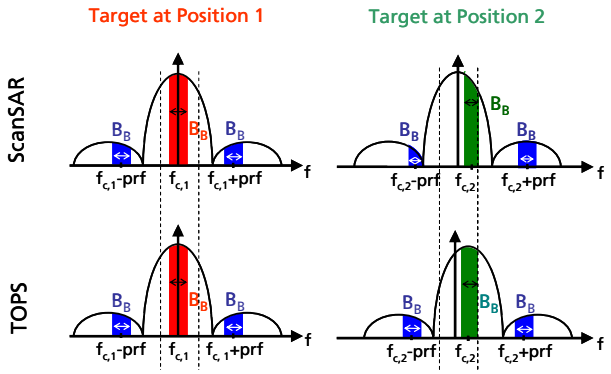

Fig. 4. Spectrum in ScanSAR (top) and TOPS (bottom) mode for different target positions corresponding to $f_{c,1}$, and $f_{c,2}$, respectively. Ambiguous bands are marked in blue.

variable target position within the burst. This position is characterized by the "target center frequency" $f_{c,t}$, which represents the mean frequency of the target echo spectrum of width B_B (cf. Fig. 4). Consequently, a variable Doppler band $B_{s,t}$ according to (1) is covered by the reflected signal.

$$B_{s,t} = \left[f_{c,t} - \frac{B_B}{2}, f_{c,t} + \frac{B_B}{2} \right] \tag{1}$$

In the following, this target position dependent echo spectrum will be investigated with respect to the frequency dependent multi-aperture processing network.

2.1 Azimuth-Ambiguity-to-Signal Ratio: $AASR_{N,B}$

As investigated in [1], the residual azimuth ambiguities in the SAR image are determined by aliasing in the originally received signal taking into account a possible amplification by the processing network filter functions $P_{j,PRF}(f)$. As the filter functions vary with Doppler frequency, the amplification of the ambiguous contribution depends on the band where it is situated. Thus, as the ambiguous bands vary with the target position (cf. Fig. 4), the resulting ambiguous power depends on $B_{s,t}$. This allows for quantifying the azimuth ambiguous energy suppression in burst mode operation ($AASR_{N,B}$) by (2), where $W(B_{s,t})$ indicates a rectangular window confining the band $B_{s,t}$.[1]

$$AASR_{N,B} = \frac{\mathrm{E}\left[\left| 2 \cdot \sum_{k=1}^{\infty} \left(U_k(f) \cdot \sum_{m=1}^{N} \sum_{j=1}^{N} H_{jk}(f) \cdot P_{jm,PRF}(f) \right) \cdot W(B_{s,t}) \right|^2 \right]}{\mathrm{E}\left[\left| U(f) \cdot W(B_{s,t}) \right|^2 \right]} \tag{2}$$

Hence, besides the varying signal power ('scalloping'), the processing of different sub-spectra corresponding to different target positions within the burst will result in a variation of the residual azimuth ambiguities of these targets. Thus, burst mode operation yields a scalloping-like effect for the $AASR_{N,B}$, both for TOPS and ScanSAR.

[1] $U(f)$ gives the SAR signal of a mono-aperture system, while $H_j(f)$ relates $U(f)$ and the signal at receiver j. $P_{jm,PRF}(f)$ represents the filter function of channel j on one of the N sub-bands m of width PRF. Further, index k indicates a frequency shift by $k \cdot PRF$ and represents the ambiguity of order k. Finally, the operator E[.] represents the mean value.

2.2 *SNR* Scaling: $\Phi_{bf,B}$ and L_p

Similar to the residual azimuth ambiguities, the noise power scaling by the processing network is governed by the target position. Thus, the expression for noise scaling in stripmap operation [1],[6], is extended by introducing the dependency on the band $B_{s,t}$ leading to $\Phi_{bf,B}$ in (3) that gives the ratio between input and output noise power, $p_{n,el}$ and $p_{n,B_{s,t}}$, respectively. Eq. (3) expresses the scalloping-like behaviour of the noise power scaling for both, TOPS and ScanSAR. Regarding the signal power, ScanSAR mode entails a loss given by L_p in (4) while TOPS ensures constant signal power, i.e. $L_p \approx 0$. The scaling of the signal-to-noise ratio (SNR) is then determined by the combination of the noise scaling in (3) with the signal variation in (4).

$$\Phi_{bf,B} := \frac{p_{n,B_{s,t}}}{p_{n,el}} = N \cdot F \cdot \sum_{j=1}^{N} \mathrm{E}\left[\left| P_{j,PRF}(f) \right|^2 \cdot W(B_{s,t}) \right] \tag{3}$$

$$L_p = \mathrm{E}\left[\left| U(f) \cdot W(B_{s,t}) \right|^2 \right] \Big/ \mathrm{E}\left[\left| U(f) \cdot rect\left(f / B_B \right) \right|^2 \right] \tag{4}$$

3. SCANSAR SYSTEM DESIGN EXAMPLE

3.1 Timing and System Parameter

The following Section presents the design of an X-band ScanSAR system capable to cover a swath of 400 km with a resolution of 5 m. Timing analysis reveals PRF values closely located from 1150 Hz up to 1240 Hz making the implementation of system optimization as described in [1] dispensable. All further requirements and parameters are summarized by Table 1.

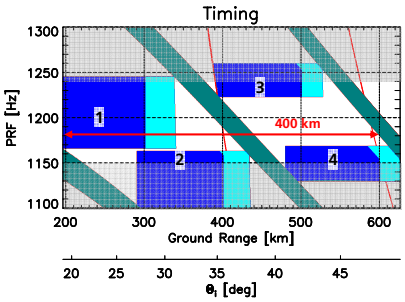

Fig. 5. Timing diagram considering transmit events (green) and nadir returns (red). 4 swaths of length 105 km each cover a ground range of 400 km.

With the aim of optimizing the spatial sampling within the range of operation, the overall azimuth dimension of the antenna is set to 12.8 m leading to an optimum PRF of ~1180 Hz. Further, a burst bandwidth of 1.2 kHz is needed to obtain a resolution of 5 m what yields a system bandwidth B_D=6 kHz. In combination with the minimum PRF, this requires a minimum of N=6 receive apertures to fulfil the Nyquist criterion. Nevertheless, N=8 is chosen as the results in [6] imply that sufficient ambiguity suppression in combination with tolerable scalloping of the signal power needs considerable oversampling. Finally, a transmit antenna length in azimuth of 2.1 m is sufficiently small to achieve with 4 bursts a resolution of 5 m but large enough to guarantee adequate ambiguity suppression (cf. Table 1).

Parameter	Symbol	Value
Carrier wavelength	λ	3.1 cm
Azimuth ambiguity suppression	$AASR_{N,B}$	≤ -20 dB
Transmit duty cycle	dc	15 %
Orbit height	h_s	630 km
Sensor velocity	v_s	7545 m/s
Subswath-width on ground	$W_{g,s}$	105 km
No. of subswaths/bursts	N_B	4
Operated *PRF* values (In order from burst 1 to 4)	PRF	1180, 1160, 1240, 1150 Hz
Rx sub-apertures in azimuth	N	8
Rx sub-aperture length in azimuth	$d_{a,rx}$	1.6 m
Tx antenna length in azimuth	$d_{a,tx}$	2.1 m
Burst bandwidth	B_B	1.2 kHz
System bandwidth in azimuth	B_D	6.0 kHz
TOPS coefficient	α	5
Overall antenna height in elevation	H_a	2 m
Applied Beamforming in Elevation		SCORE
Transmit antenna size in elevation	$d_{el,tx}$	0.19–0.31 m
System temperature	T	300 K
Losses (azimuth, atmospheric, system, Rx noise, 2-way)	$L{\cdot}F$	5.9 dB

TABLE 1. System parameters.

3.2 TOPS

In the frame of the above design example, additionally the TOPS mode is applied straight-forwardly to the derived system with a coefficient of α =5 and assuming an optimum steered pattern not taking into account any single element characteristic or grating lobes. It is worth noting that the design is adapted to ScanSAR and consequently the results do not represent a fair comparison between TOPS and ScanSAR. Nevertheless, the obtained performance gives first hints about the potential and challenges of multi-channel TOPS systems.

3.3 Performance Analysis

In the following, system performance is evaluated by simulations carried out for point-like targets. The analysis comprises the characteristics of azimuth resolution, azimuth-ambiguity suppression, scalloping of signal power and noise scaling factor Φ_{bf} versus the "target center frequency" $f_{c,t}$ (cf. Fig. 6 to Fig. 9). Where necessary, all four sub-swaths are considered.

3.3.1 Geometric Resolution in Azimuth: δ_{az}

A constant azimuth resolution of 5 m or better is achieved for all sub-swaths of the ScanSAR system, while the TOPS mode yields a slight increase up to ~5.5 m (cf. Fig. 6). This degradation is due to the effectively shrunk pattern of the TOPS mode and can be avoided by a specific system design. Note that the resolution in TOPS is constant as an optimum steered pattern is assumed. The variations in Fig. 6 on the right are only caused by numerics. In contrast, the decay of the pattern with increasing $f_{c,t}$ in ScanSAR leads to a slight increase of the resolution which is negligible.

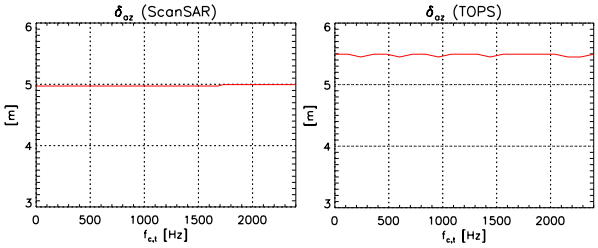

Fig. 6. δ_{az} vs. $f_{c,t}$ for ScanSAR (left) and TOPS (right).

3.3.2 Azimuth-Ambiguity-to-Signal Ratio: $AASR_{N,B}$

Fig. 7 shows the suppression of azimuth ambiguous energy by ScanSAR (left) and TOPS (right) for all four subswaths. In the ScanSAR system the suppression worsens with increasing center frequency $f_{c,t}$ caused by the decreasing signal power due to the pattern decay (cf. Fig. 4) and the increasingly unfavourable scaling of ambiguous energy by the multi-aperture processing. In the worst case, still a suppression of better than -21dB is ensured. In contrast, TOPS mode allows for avoiding the effect of the antenna pattern and is only influenced by the processing network as can be seen from the constant solid red line in the right plot of Fig. 7, left, that corresponds to uniform sampling. In reverse, the other characteristics of Fig. 7, right (dotted, dashed, dotted dashed), show the scalloping introduced by the multi-aperture processing for the respective *PRF*. Especially for large values of $f_{c,t}$ the processing network introduces a clear degradation of the $AASR_{N,B}$.

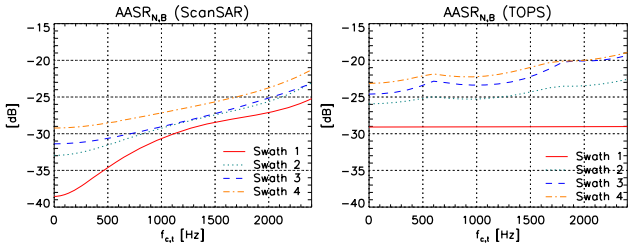

Fig. 7. $AASR_{N,B}$ vs. $f_{c,t}$ for ScanSAR (left) and TOPS (right) operation. Results for all four sub-swaths indicated by different line styles and colours.

In comparison to ScanSAR, the degradation is worse for TOPS as the steered pattern is more sensitive to the multi-aperture processing in terms of azimuth ambiguities. This is caused by the shifted pattern that results in more spectral energy situated outside the system band [$-N{\cdot}PRF/2$, $N{\cdot}PRF/2$] and giving rise to ambiguities.

3.3.3 Noise Scaling Factor Φ_{bf} and NESZ

In order to derive the *NESZ* of the systems, firstly the normalized loss of signal power, L_p, is determined. Fig. 8, left, shows the result for the ScanSAR system with a maximum power loss of ~2.65 dB. As expected, no scalloping is encountered in TOPS mode as an optimum steered pattern is assumed. In reality, the single element pattern of the array antenna causes a small scalloping effect.

Next, the *SNR* scaling introduced by the digital processing network is determined considering the case where multiple separate sub-bands are focused and equation (3) is valid.

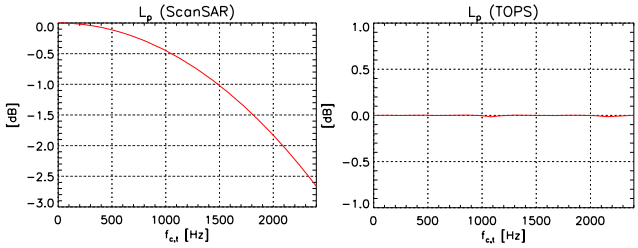

Fig. 8. L_p vs. $f_{c,t}$ for ScanSAR (left) and TOPS (right).

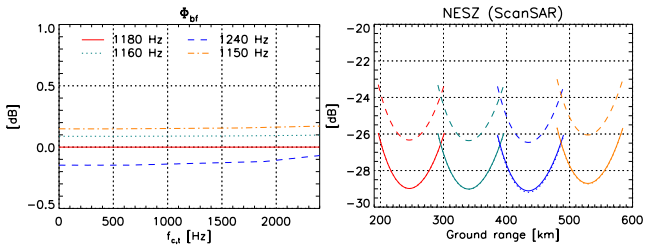

Fig. 9. Left: *SNR* scaling factor Φ_{bf} vs. $f_{c,t}$ for all sub-swaths taking into account the respective *PRF*. Right: *NESZ* vs. ground range for ScanSAR, varying from worst case (dashed lines) to best case (solid lines) and TOPS (solid lines).

Hence, both for TOPS and ScanSAR, Φ_{bf} shows a scalloping-like effect for each of the swaths as shown in Fig. 9, left. In the present case an uncritical maximum degradation of the *SNR* of ~0.2 dB is caused by the processing network (cf. Fig. 9, dotted dashed orange line). Taking now into account the system parameters given by Table 1 and including the above results for L_p and Φ_{bf} yields the system *NESZ* in Fig. 9, right. The solid line represents the *NESZ* for any target in TOPS mode and the optimum value in ScanSAR obtained for targets at $f_{c,t}$=0. The dashed line considers the worst case regarding the loss of signal power for targets at the edges of the antenna pattern in ScanSAR operation. In any case the *NESZ* is below -24 dB.

3.4 Optimized TOPS Squinted Processing

In conventional operation, the burst length in TOPS was chosen to ensure an overall bandwidth equal to the band $N{\cdot}PRF$ covered by the reconstruction filters (cf. Fig. 10, left and middle). As shown in Fig. 7, right, this entails a strong degradation of the ambiguity suppression especially for high frequencies $f_{c,t}$. The basic idea to solve this inconvenience is to vary the processing filters with the target position by centering the reconstructed band around a frequency $f_c(t)$ which is matched to the instantaneous bandwidth of the TOPS signal (cf. Fig. 10, right). In contrast to the conventional straight-forward approach, this enables longer bursts by the reconstruction of spectral components from higher squint angles. In a first try, the reconstructed bandwidth is kept constant to $N{\cdot}PRF$ and center frequencies of $k{\cdot}PRF$, k integer, were set, i.e. $f_c(t)=k{\cdot}PRF$ was chosen to minimize the offset to the actual target center frequency. Results in Fig. 11, right, show a clearly improved $AASR_{N,B}$ of better than -22 dB, where scalloping occurs only with a period of *PRF* before "switching" to the new

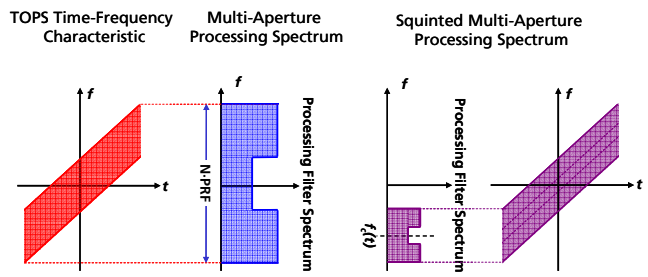

Fig. 10. TOPS time-frequency band (left), spectrum of conventional multi-aperture processing (middle) and spectrum of "squinted" processing with adaptively centered reconstructed band to ideally cover the necessary signal spectrum (right).

center frequency. The "conventional" straight-forward approach (Fig. 11, left) yields identical results within the first interval [*-PRF/2, PRF/2*] but deviates for higher $f_{c,t}$.
Further optimization could comprise an adaptation of the reconstructed bandwidth reducing the number of needed channels and a finer or even continuous adaptation of $f_c(t)$.

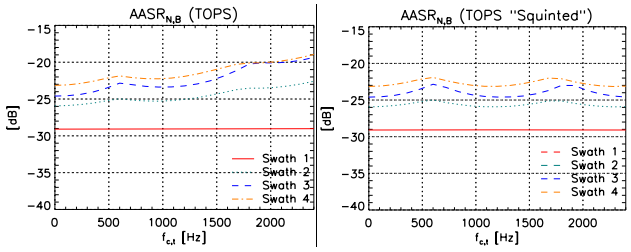

Fig. 11. TOPS mode $AASR_{N,B}$ vs. $f_{c,t}$ for conventional (left) and for adapted reconstruction with a time-varying squint (right).

4. SUMMARY

In the frame of advanced concepts for ultra-wide-swath SAR imaging [2] multi-channel systems in burst mode operation were introduced and investigated. The burst mode-inherent influence of the target position on the received signal spectrum leads to a scalloping-like effect introduced by the Doppler frequency dependent multi-channel processing. In this context, analytic description of performance figures like $AASR_N$ and *SNR* scaling was extended to burst mode operation, considering the dependency on the targets position which occurs for both, ScanSAR and TOPS mode. Further, a ScanSAR system design example demonstrated the applicability of multi-aperture signal processing in burst mode operation what enabled the imaging of an ultra-wide-swath of 400 km with a geometric resolution of 5 m. Then, TOPS mode was applied in a straight-forward approach to the ScanSAR design indicating a higher sensitivity of the steered pattern to the applied multi-channel processing with regard to residual azimuth ambiguities. Finally, an optimized processing approach adapted to TOPS was presented that yields improved performance by a time-varying squinted multi-aperture reconstruction.

5. REFERENCES

[1] N. Gebert, G. Krieger, A. Moreira, "Digital Beamforming on Receive: Techniques and Optimization Strategies for High-Resolution Wide-Swath SAR Imaging", *IEEE Trans. Aerospace and Electronic Systems*, accepted for publication.

[2] G. Krieger, et al., „Advanced Concepts for Ultra-Wide-Swath SAR Imaging with High Azimuth Resolution", *Proceedings of EUSAR*, Friedrichshafen, Germany, 2008.

[3] K. Tomiyasu, "Conceptual performance of a satellite borne, wide swath synthetic aperture radar", *IEEE Trans. Geoscience and Remote Sensing*, vol. 19, pp. 108-116, 1981.

[4] R. K. Moore, J. P. Claassen, Y. H. Lin, "Scanning spaceborne synthetic aperture radar with integrated radiometer", *IEEE Trans. Aerospace and Electronic Systems*, vol. 17, pp. 410-421, 1981.

[5] F. De Zan, A.M. Monti Guarnieri, "TOPSAR: Terrain Observation by Progressive Scans", *IEEE Trans. Geoscience and Remote Sensing*, vol. 44, pp. 2352 – 2360, 2006.

[6] N. Gebert, G. Krieger, A. Moreira, „Multi-channel ScanSAR for High-Resolution Ultra-Wide-Swath SAR Imaging", *Proceedings of EUSAR*, Friedrichshafen, Germany, 2008.